Evaluation of the Eshelby solution for the ellipsoidal inclusion and heterogeneity

Chunfang Meng *, Will Heltsley, David D. Pollard

Department of Geological and Environmental Sciences, Stanford University, Stanford, CA 94305-2115, USA

ARTICLE INFO

ABSTRACT

We present a MATLAB code that evaluates the quasi-static elastic displacement strain and stress fields for the ellipsoidal inclusion and heterogeneity, the Eshelby solution. We first give an introduction to the underlaying inclusion problem. Then we describe the Eshelby solution for the elastic field inside and outside an ellipsoidal inclusion. We introduce the equivalency between the inclusion and inhomogeneity problems and elaborate the code's functionalities. Finally, we make the ellipsoidal inclusion undergo a series of geometrical transformations to emulate a spheroid inclusion, a 2D elliptical void, and a planar crack for which the surrounding elastic field is either known or accurately approximated. By comparing the Eshelby solution against those *known* solutions, we conclude that the code is valid. By these emulations, we show that the Eshelby solution can encompass many special problems in a unified form.

1. Introduction

The elastic fields surrounding and inside an inhomogeneity have many applications in the material and geological sciences. For an ellipsoidal inhomogeneity in an isotropic infinite body, the elastic field was formulated by Eshelby (1957, 1959, 1961) with an equivalent inclusion problem (Mura, 1987, p. 179). Rudnicki (1977) used the Eshelby solution to investigate the inception of faulting. Eidelman and Reches (1992) used the solution to interpret the tectonic stress state from fracture patterns in pebbles embedded in a conglomerate. Sharma and Ganti (2004) modified the original solution to simulate nanoinclusions. Jiang (2007) used the solution to model viscous objects in a Newtonian fluids with different viscosities when solving for the preferred orientation fabric in igneous and metamorphic rocks. Katsman (2010) used the solution to model compaction bands in 2D.

The Eshelby solution for an arbitrary ellipsoidal inclusion (inhomogeneity) requires extensive calculations, so Healy (2009) and Reches (1998) evaluated the simplified solutions for the spheroidal inhomogeneities, where the semiaxes are $a_1 = a_2 \neq a_3$.

We developed a MATLAB code that evaluates the strain, stress, and displacement fields inside and outside a *general* ellipsoidal inclusion or inhomogeneity.

2. Inclusions and eigenstrains

The inclusion problem described by Eshelby (1957) is as follows: A region (inclusion) in an infinite homogeneous, isotropic, and linear elastic medium (matrix) undergoes a change in shape and size. Under the constraint of the matrix, the inclusion has an arbitrary homogeneous strain. Our objective is to evaluate the elastic fields of the inclusion and matrix.

The definition of eigenstrain, ϵ^*, summarized by Mura (1987, p. 1), can be regarded as the strain state that the inclusion will enter if we remove the constraint of the matrix. Eshelby (1957) referred to this as *stress-free strain*.

In Mura (1987), an inclusion is defined as a subdomain Ω in a domain D, and eigenstrain $\epsilon^*_{ij}(x)$ is given in Ω and zero in $D-\Omega$. The elastic moduli in the inclusion Ω and the matrix $D-\Omega$ are the same. The displacement u_j, strain ϵ_{ij}, and stress σ_{ij} for both the inclusion and matrix are expressed (Mura, 1987, p. 11) as

$$u_i(\mathbf{x}) = -C_{kjmn} \int_\Omega \epsilon^*(\mathbf{x}')G_{ij,k}(\mathbf{x}-\mathbf{x}')\,d\mathbf{x}', \tag{1}$$

$$\epsilon_{ij}(\mathbf{x}) = -\frac{1}{2}\int_\Omega C_{klmn}\epsilon^*_{mn}(\mathbf{x}')(G_{ik,lj}(\mathbf{x}-\mathbf{x}')+G_{jk,li}(\mathbf{x}-\mathbf{x}'))\,d\mathbf{x}', \tag{2}$$

$$\sigma_{ij}(\mathbf{x}) = -C_{ijkl}\left(\int_\Omega C_{pqmn}\epsilon^*_{mn}(\mathbf{x}')G_{kp,ql}(\mathbf{x}-\mathbf{x}')\,d\mathbf{x}' + \epsilon^*_{kl}(\mathbf{x})\right), \tag{3}$$

where C_{ijkl} is the stiffness tensor; G_{ij} is Green's function; and $\mathbf{x}$ is the position vector; and $\mathbf{x}'$ denotes the position of a point source.

* Corresponding author.
E-mail addresses: chunfang@stanford.edu (C. Meng), dpollard@stanford.edu (D.D. Pollard).

3. Ellipsoidal inclusion in an isotropic infinite matrix

An ellipsoidal inclusion Ω with semiaxis a_j in an infinite isotropic elastic body D has equation

$$\frac{x_1^2}{a_1^2} + \frac{x_2^2}{a_2^2} + \frac{x_3^2}{a_3^2} \leq 1. \tag{4}$$

The coordinates x_1, x_2, x_3 are equivalent to x, y, z in later sections.

For isotropic materials, Green's function is given (Mura, 1987, p. 22) by

$$G_{ij}(\mathbf{x}-\mathbf{x}') = \frac{1}{16\pi\mu(1-v)|\mathbf{x}-\mathbf{x}'|}\left((3-4v)\delta_{ij} + \frac{(x_i-x_i')(x_j-x_j')}{|\mathbf{x}-\mathbf{x}'|^2}\right). \tag{5}$$

Assuming the eigenstrain in the inclusion is a constant, we can take ϵ^* out of the integrals of Eqs. (1)–(3). Eshelby (1957, 1959, 1961) derived impressive solutions for the interior and exterior elastic field of such an inclusion. One of Eshelby's prominent results is that the strain and stress fields within the inclusion are uniform,

$$\epsilon_{ij} = S_{ijkl}\epsilon_{kl}^* \quad \text{for } \mathbf{x} \in \Omega, \tag{6}$$

where S_{kl} is called the Eshelby tensor (Mura, 1987, p. 77),

$$S_{ijkl} = S_{jikl} = S_{ijlk},$$

$$S_{1111} = \frac{3}{8\pi(1-v)}a_1^2 I_{11} + \frac{1-2v}{8\pi(1-v)}I_1,$$

$$S_{1122} = \frac{1}{8\pi(1-v)}a_2^2 I_{12} - \frac{1-2v}{8\pi(1-v)}I_1,$$

$$S_{1133} = \frac{1}{8\pi(1-v)}a_3^2 I_{13} - \frac{1-2v}{8\pi(1-v)}I_1,$$

$$S_{1212} = \frac{a_1^2+a_2^2}{16\pi(1-v)}I_{12} + \frac{1-2v}{16\pi(1-v)}(I_1+I_2), \tag{7}$$

where v is Poisson's ratio; I_i and I_{ij} are given by integrals, Routh (1895),

$$I_1 = 2\pi a_1 a_2 a_3 \int_0^\infty \frac{ds}{(a_1^2+s)\Delta(s)},$$

$$I_{11} = 2\pi a_1 a_2 a_3 \int_0^\infty \frac{ds}{(a_1^2+s)^2\Delta(s)},$$

$$I_{12} = 2\pi a_1 a_2 a_3 \int_0^\infty \frac{ds}{(a_1^2+s)(a_2^2+s)\Delta(s)}, \tag{8}$$

where $\Delta(s) = (a_1^2+s)^{1/2}(a_2^2+s)^{1/2}(a_3^2+s)^{1/2}$; s is the integration variable. The remaining I_i and I_{ij} are found by synchronized cyclic permutations of 1,2,3 and a_1, a_2, a_2.

For $a_1 > a_2 > a_3$, the I_i can be expressed by standard elliptical integrals (Gradshteyn and Ryzhik, 1965),

$$I_1 = \frac{4\pi a_1 a_2 a_3}{(a_1^2-a_2^2)(a_1^2-a_3^2)^{1/2}}(F(\theta,k)-E(\theta,k)),$$

$$I_3 = \frac{4\pi a_1 a_2 a_3}{(a_2^2-a_3^2)(a_1^2-a_3^2)^{1/2}}\left(\frac{a_2(a_1^2-a_3^2)^{1/2}}{a_1 a_3} - E(\theta,k)\right), \tag{9}$$

where

$$F(\theta,k) = \int_0^\theta \frac{dw}{(1-k^2\sin^2 w)^{1/2}},$$

$$E(\theta,k) = \int_0^\theta (1-k^2\sin^2 w)^{1/2}\, dw,$$

$$\theta = \arcsin(1-a_3^2/a_1^2)^{1/2},$$

$$k = ((a_1^2-a_2^2)/(a_1^2-a_3^2))^{1/2}. \tag{10}$$

Among I_i and I_{ij} we have relations (Mura, 1987),

$$I_1+I_2+I_3 = 4\pi,$$

$$3I_{11}+I_{12}+I_{13} = 4\pi/a_1^2,$$

$$3a_1^2 I_{11}+a_2^2 I_{12}+a_3^2 I_{13} = 3I_1,$$

$$I_{12} = (I_2-I_1)/(a_1^2-a_2^2). \tag{11}$$

With these relations and their cyclic counterparts, I_1 and I_3 from Eq. (9) are sufficient to express the other I_i and I_{ij}.

In later sections, we employ a numerical routine **elliptic12** by Igor (2005) to approximate the elliptical integral in Eq. (10) with tolerance of order 10^{-16}. This means that the solutions we present are not analytical (exact) in the strict sense. We refer to this method as quasi-analytical.

For the exterior elastic field (Mura, 1987),

$$\epsilon_{ij}(\mathbf{x}) = D_{ijkl}(\mathbf{x})\epsilon_{kl}^* \quad \text{for } \mathbf{x} \in D-\Omega, \tag{12}$$

where

$$
\begin{aligned}
8\pi(1-v)D_{ijkl}(x) = &\; 8\pi(1-v)S_{ijkl}(\lambda) + 2v\delta_{kl}x_i I_{I,j}(\lambda) \\
&+ (1-v)(\delta_{il}x_k I_{K,j}(\lambda)+\delta_{jl}x_k I_{K,i}(\lambda) \\
&+ \delta_{ik}x_l I_{L,j}(\lambda)+\delta_{jk}x_l I_{L,i}(\lambda)) \\
&- \delta_{ij}x_k(I_K(\lambda)-a_I^2 I_{KI}(\lambda))_{,l} \\
&- (\delta_{ik}x_j+\delta_{jk}x_i)(I_J(\lambda)-a_I^2 I_{IJ}(\lambda))_{,l} \\
&- (\delta_{il}x_j+\delta_{jl}x_i)(I_J(\lambda)-a_I^2 I_{IJ}(\lambda))_{,k} \\
&- x_i x_j(I_J(\lambda)-a_I^2 I_{IJ}(\lambda))_{,lk}.
\end{aligned}
\tag{13}
$$

The upper case indices take the values of the corresponding lower case indices, but only repeated lower case indices are summed over. δ_{ij} is the Dirac delta function. λ is the largest positive root of

$$\frac{x_1^2}{a_1^2+\lambda} + \frac{x_2^2}{a_2^2+\lambda} + \frac{x_3^2}{a_3^2+\lambda} = 1 \tag{14}$$

for $\mathbf{x} \in D-\Omega$ and zero for $\mathbf{x} \in \Omega$. $I_{i(j)}(\lambda)$ are defined by Eq. (8) with the lower integral limits replaced by λ. $S_{ijkl}(\lambda)$ are given by Eq. (7) for corresponding $I_{i(j)}(\lambda)$.

To solve $D_{ijkl}(x)$ in Eq. (13), we need $I_i(\lambda)$, $I_{ij}(\lambda)$ and their first and second-order derivatives with respect to x_i. The $I_i(\lambda)$ and $I_{ij}(\lambda)$, similarly to Eqs. (9)–(11), become

$$I_1(\lambda) = \frac{4\pi a_1 a_2 a_3}{(a_1^2-a_2^2)(a_1^2-a_3^2)^{1/2}}(F(\theta(\lambda),k)-E(\theta(\lambda),k)),$$

$$I_3(\lambda) = \frac{4\pi a_1 a_2 a_3}{(a_2^2-a_3^2)(a_1^2-a_3^2)^{1/2}}\left(\frac{(a_2^2+\lambda)(a_1^2-a_3^2)^{1/2}}{\prod_k(a_k^2+\lambda)^{1/2}} - E(\theta(\lambda),k)\right),$$

$$I_2(\lambda) = \frac{4\pi a_1 a_2 a_3}{\prod_k(a_k^2+\lambda)^{1/2}} - I_1(\lambda) - I_3(\lambda),$$

$$I_{ij}(\lambda) = -\frac{I_i(\lambda)-I_j(\lambda)}{a_i^2-a_j^2} \quad \text{for } i \neq j,$$

$$I_{ii}(\lambda) = \frac{4\pi a_1 a_2 a_3}{3(a_i^2+\lambda)\prod_k(a_k^2+\lambda)^{1/2}} - \frac{\sum_j I_{ij}(\lambda)}{3}, \tag{15}$$

where $\prod$ is the sign of the factorial, $F(\theta(\lambda),k)$ and $E(\theta(\lambda),k)$, are given by Eq. (10), with parameter θ modified (Gradshteyn and Ryzhik, 1965):

$$\theta = \arcsin\left(\frac{a_1^2-a_3^2}{a_1^2+\lambda}\right)^{1/2}. \tag{16}$$

Facilitated by (Mura, 1987, 11.40.1–11.40.4), we can express the first- and second-order derivatives of I_i and I_{ij} in terms of λ's

derivatives:

$$I_{i,j} = \frac{-2\pi a_1 a_2 a_3}{(a_i^2 + \lambda)\prod_m(a_m^2 + \lambda)^{1/2}} \lambda_{,j},$$

$$I_{ij,k} = \frac{-2\pi a_1 a_2 a_3}{(a_i^2 + \lambda)(a_j^2 + \lambda)\prod_m(a_m^2 + \lambda)^{1/2}} \lambda_{,k},$$

$$I_{i,jk} = \frac{-2\pi a_1 a_2 a_3}{(a_i^2 + \lambda)\prod_m(a_m^2 + \lambda)^{1/2}} \left(\lambda_{,jk} - \left(\frac{1}{a_i^2 + \lambda} + \frac{1}{2}\sum_n \frac{1}{a_n^2 + \lambda} \right) \lambda_{,j}\lambda_{,k} \right),$$

$$I_{ij,kl} = \frac{-2\pi a_1 a_2 a_3}{(a_i^2 + \lambda)(a_j^2 + \lambda)\prod_m(a_m^2 + \lambda)^{1/2}} \left(\lambda_{,kl} - \left(\frac{1}{a_i^2 + \lambda} + \frac{1}{a_j^2 + \lambda} + \frac{1}{2}\sum_n \frac{1}{a_n^2 + \lambda} \right) \lambda_{,k}\lambda_{,l} \right).$$

$$(17)$$

From Eq. (14), we have the first- and second-order derivatives of $\lambda(x)$,

$$\lambda_{,i} = \frac{2x_i}{(a_I^2 + \lambda)} \bigg/ \frac{x_j x_j}{(a_j^2 + \lambda)^2}, \quad \lambda_{,ij} = \frac{F_{i,j} - \lambda_{,i}C_j}{C}, \quad (18)$$

where

$$F_i = \frac{2x_i}{a_I^2 + \lambda}, \quad C = \frac{x_i x_i}{(a_I^2 + \lambda)^2}. \quad (19)$$

Substituting Eqs. (15), (17), and (18) into Eq. (13), we have expressions for $D_{ijkl}(x)$.

For a given eigenstrain ϵ_{ij}^*, we have *quasi-analytical* expressions for the strain fields for both the inclusion equation (6) and the matrix equation (12). Multiplying the strain by the stiffness matrix C_{ijkl}, we have the corresponding stress field

$$\sigma_{ij} = C_{ijkl}\epsilon_{kl}(x). \quad (20)$$

Because ϵ_{ij} in Ω is uniform, σ_{ij} in Ω is also uniform.

The displacement field is given by Mura (1987, 11.30) as

$$u_i(x) = \frac{1}{8\pi(1-v)} (\psi_{,jli}\epsilon_{jl}^* - 2v\epsilon_{mm}^*\phi_{,i} - 4(1-v)\epsilon_{il}^*\phi_{,l}), \quad (21)$$

where ϕ and ψ are defined by

$$\phi(x) = \int_\Omega |x - x'|\, dx',$$

$$\psi(x) = \int_\Omega \frac{1}{|x - x'|}\, dx'. \quad (22)$$

The functions ϕ and $\psi_{,i}$, defined by Ferrers (1877) and Dyson (1981), can be expressed in terms of $I_i(\lambda)$ and $I_{ij}(\lambda)$,

$$\phi = \tfrac{1}{2}(I(\lambda) - x_n x_n I_N(\lambda)),$$

$$\psi_{,i} = \tfrac{1}{2}x_i(I(\lambda) - x_n x_n I_N(\lambda) - a_I^2(I_I(\lambda) - x_n x_n I_{IN}(\lambda)), \quad (23)$$

where

$$I = \frac{4\pi a_1 a_2 a_3 F(\theta(\lambda), k)}{(a_1^2 - a_3^2)^{1/2}}. \quad (24)$$

Facilitated by Mura (1987, 11.40.4),we express $\phi_{,i}$ and $\psi_{,ijl}$, in terms of I_i, I_{ij}, and their first-order derivatives:

$$\phi_{,i} = -x_i I_I(\lambda),$$

$$\psi_{,ijl} = -\delta_{ij}x_l(I_L(\lambda) - a_I^2 I_{IL}(\lambda)) - x_i x_j(I_J(\lambda) - a_I^2 I_{IJ}(\lambda))_{,l}$$
$$\quad - (\delta_{il}x_j + \delta_{jl}x_i)(I_J(\lambda) - a_I^2 I_{IJ}(\lambda)). \quad (25)$$

Substituting Eqs. (25), (15), (17), and (18) into Eq. (21), we have *quasi-analytical* expressions for the displacement fields $u_i(x)$ for both the inclusion and the matrix.

4. Equivalent inclusion method

Suppose the elastic field we would like to evaluate is characterized by different elastic moduli of the subdomain and matrix, i.e., C_{ijkl}^* in Ω and C_{ijkl} in $D-\Omega$. Also, instead of beams stress-free at infinity, the matrix is subjected to remote homogeneous stress σ_{ij}^∞. This makes the problem, referred to as the *inhomogeneity problem*, different from the *inclusion problem* in previous sections. Eshelby (1957) first argued that the stress perturbation of a homogeneous applied stress due to the presence of an ellipsoidal inhomogeneity can be determined by an inclusion problem when the eigenstrain is chosen properly. This is called the *equivalent inclusion* method.

To solve for the *fictitious* eigenstrain ϵ_{ij}^*, we rewrite Mura (1987, 22.13),

$$(\Delta C_{ijkl}S_{klmn} - C_{ijmn})\epsilon_{mn}^* = -\Delta C_{ijkl}\epsilon_{kl}^\infty - C_{ijkl}^*\epsilon_{kl}^P, \quad (26)$$

where $\Delta C_{ijkl} = C_{ijkl} - C_{ijkl}^*$; and from the relation $\sigma_{ij}^\infty = C_{ijkl}\epsilon_{ij}^\infty$, we have the remote strain ϵ_{ij}^∞. ϵ_{ij}^p is an arbitrary eigenstrain that the inhomogeneity was initially subjected to.

We have stress and strain fields as follows (Mura, 1987, 22.8–22.13):

$$\epsilon_{ij} = \epsilon_{ij}^\infty + S_{ijmn}\epsilon_{mn}^*,$$

$$\sigma_{ij} = \sigma_{ij}^\infty + C_{ijkl}(S_{klmn}\epsilon_{mn}^* - \epsilon_{mn}^*) \quad \text{in } \Omega,$$

$$\epsilon_{ij}(\mathbf{x}) = \epsilon_{ij}^\infty + D_{klmn}(\mathbf{x})\epsilon_{mn}^*,$$

$$\sigma_{ij}(\mathbf{x}) = \sigma_{ij}^\infty + C_{ijkl}D_{klmn}(\mathbf{x})\epsilon_{mn}^* \quad \text{for } \mathbf{x} \in D-\Omega. \quad (27)$$

Note that the eigenstrain is *stress-free*, so we subtract it from the total strain when calculating the stress in the inhomogeneity. And, since the exterior is free from eigenstrain, we have the elastic stress–strain correspondence.

Displacement $u_i(x)$ is calculated by Eq. (21) for the eigenstrain ϵ_{ij}^*. The displacement here is equivalent to the displacement perturbation caused by the inhomogeneity and does not include the displacement due to the σ_{ij}^∞.

5. Formulate the solution with MATLAB

We use a *main* script, **incl_prob**, to handle the input data structure, call the Eshelby solver, **Esh_sol**, and present the results.

The input structure *incl* has attributions

- *Em* Young's modulus of the matrix,
- *vm* Poisson ratio of the matrix;
- *Eh* Young's modulus of the inhomogeneity;
- *vh* Poisson ratio of the inhomogeneity;
- *dim* the ellipsoidal dimensions a_i;
- *ang* rotation angles around coordinate axes;
- *stressvec* remote stress σ_{ij}^∞;
- *eigp* initial eigenstrain ϵ_{ij}^p;
- *grid* observation grid(s) where we evaluate the solutions,

where the stress and strain tensors are in the form of six-component vectors because of the symmetry.

The **Esh_sol** function reads the input data and output arguments, "disp," "stress," and "strain." The outputs are evaluated on the observation grid(s) for the specified output arguments. We elaborate the routines called by this function in the order of appearance:

Ctensord constructs the stiffness tensors C_{ijkl} and C_{ijkl}^* for given elastic moduli (*Em*, *vm*) and (*Eh*, *vh*). From the stress–strain correspondence, Eq. (20), we calculate the remote strain ϵ_{ij}^∞ for

the remote stress σ_{ij}^{∞}. Note that if $C_{ijkl} = C_{ijkl}^{*}$, $\sigma_{ij}^{\infty} = 0$ and $\epsilon_{ij}^{p} \neq 0$, we have the *original* inclusion problem.

Esh_int constructs the Eshelby tensor S_{ijkl} for a given *vm* and ellipsoid dimension a_i using Eqs. (7)–(11). With $C_{ijkl}^{(*)}$, ϵ_{ij}^{∞}, and S_{ijkl} we calculate the *fictitious* eigenstrain ϵ_{ij}^{*} by Eq. (26).

Esh_D4 constructs the tensor $D_{ijkl}(x)$ by Eqs. (13)–(18) for given *vm*, a_i and coordinates x_i. With $D_{ijkl}(\mathbf{x})$, we calculate the exterior strain and stress by Eq. (27).

Esh_disp constructs the displacements u_i by Eqs. (21)–(25) for given *vm*, a_i, x_i, and ϵ_{ij}^{*}.

Esh_D4_disp merges the functionalities of **Esh_D4** and **Esh_disp**.

Because the displacements, $u_i(\mathbf{x})$, require different-order derivatives of $I_{i(j)}$, Eq. (17), than the strain ϵ_{ij}, or stress, Eq. (12), we choose a routine among **Esh_D4**, **Esh_disp**, and **Esh_D4_disp** to calculate the outputs efficiently. For example, if only "disp" appears in the output arguments, **Esh_sol** will only call **Esh_disp**. Therefore the code runs faster for fewer outputs.

At the end of **incl_prob**, we selectively plot the outputs for given observation grids.

6. Validate the code

We first demonstrate the exterior strain perturbation caused by an ellipsoidal inclusion ($C_{ijkl} = C_{ijkl}^{*}$) with a given eigenstrain $\epsilon_{ii}^{*} = 10^{-3}$ and $\epsilon_{ij} = 0$ for $i \neq j$. We let the ellipsoid's axis ratio a_y/a_x vary from 0.01 to 100 to show its impact on the exterior elastic field.

Note, we denote the semiaxes with subscript x,y,z, equivalent to the index 1, 2, 3 in the previous section, meaning that the ellipsoid is *standard*; i.e., semiaxes overlap with the coordinate axes. The code, however, allows one to have oblique ellipsoid, without the limitation $a_1 > a_2 > a_3$ required by Eq. (9).

We observe the exterior along the x-axis, $x \in [2,10]$, and evaluate tension in y. The results are plotted in Fig. 1.

As shown, when $a_y/a_x \ll 1$, the strain concentrates in the vicinity of the inclusion tip as if the exterior is adjacent to a fracture. When $a_y/a_x \gg 1$, the strain distribution becomes flat, as if the exterior is pushed by the plane.

The method we employ to validate the code is to transform the ellipsoid into some less general shapes for which the surrounding elastic fields are known or accurately approximated by others.

Instead of for the *inclusion* problem as shown above, we found *known* solutions for the inhomogeneity problems; i.e., $C_{ijkl} \neq C_{ijkl}^{*}$ with remote stress σ_{ij}^{∞}. For comparison, we keep the inhomogeneity free from initial eigenstrain; i.e., $\epsilon_{ij}^{p} = 0$ in Eq. (26). Because of the equivalence mentioned in the previous section, once we validate the solution for the inhomogeneity problem, we also validate the solution for the original inclusion problem. And because the inhomogeneity problem with initial eigenstrain is solved by superposition of the inclusion and eigenstrain-free inhomogeneity problems, we ultimately validate the code in general.

From the general ellipsoid, i.e., $a_x \neq a_y \neq a_z$, we gradually make two of the semiaxes equal, $a_z \to a_y$. During this process, we evaluate a series of solutions on a fixed observation route. For the spheroid, $a_x \neq a_y = a_z$, inhomogeneity, the Eshelby solution is given by Healy (2009). In the process, we would expect the elastic field to approach and finally equal Healy's solution. From there, we continue the transformation trend so the spheroid becomes a different ellipsoid. The elastic field should then gradually differ from Healy's solution.

We set the ellipsoid geometry: $a_x = 0.1$, $a_y = 1$, and a_z, sweeps from 0.25 to 4. When a_z reaches 1, the ellipsoid becomes a spheroid and the result should reproduce Healy's unmodified MATLAB code. Like Healy (2009), we also set the ellipsoid as a void, i.e., $Eh = 0$, $vh = 0$, and remote stress $\sigma_{xx}^{\infty} = 10^{6}$, other components zero. Here we leave out all the units. One may follow SI or any other consistent system to give these values physical meaning. We evaluate the elastic field along the route $y = 0.4$, $z = 0.4$, and $x \in [0, 2.5]$. Note that we keep the route offset from the origin
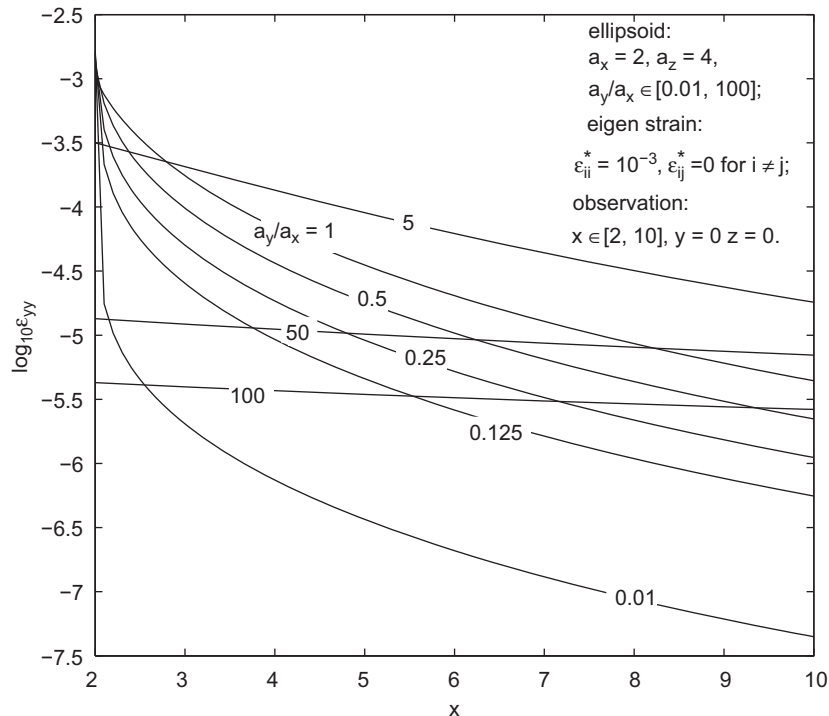

Fig. 1. Strain perturbation for ellipsoidal inclusions with different a_x/a_y.

to make the case a bit more general. The results are plotted in Fig. 2.

As a_z increases, the ellipsoid starts to intercept the observation route. Since the ellipsoid is void, i.e., traction-free, the stress drops steeply to zero at the interface. When the geometry becomes spheroidal, the stress reproduces Healy's solution, suggesting that the calculations are consistent. When the geometry deviates from a spheroid, the stress differs gradually from Healy's solution.

Let us make another comparison before we claim that the code is valid. For the ellipsoid, $a_x=0.1$, $a_y=1$, we *stretch* it on the a_z semiaxis to about order 10^3 of the other two. When we look at it from the $z=0$ plane, the ellipsoid is evolving into an elliptical cylinder. At places close to the $z=0$ plane, the z coordinate becomes less relevant to the elastic field than the x, y coordinates, so we have degenerated the 3D problem to a 2D problem. For a 2D elliptical void in an infinite elastic body, Muskhelishvili (1953)
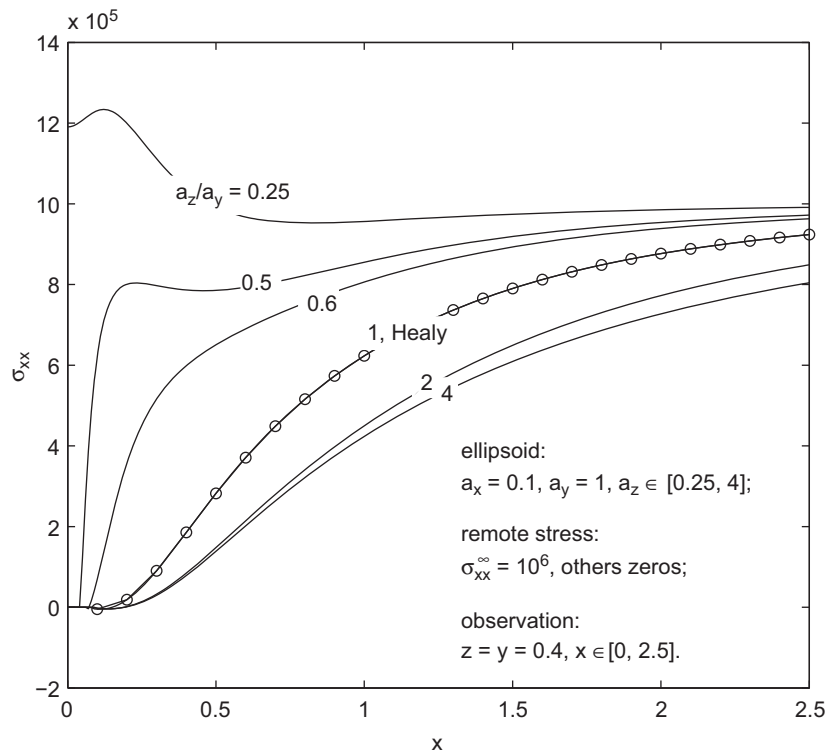

Fig. 2. Stress evolution as an ellipsoid approaches and deviates from a spheroid.
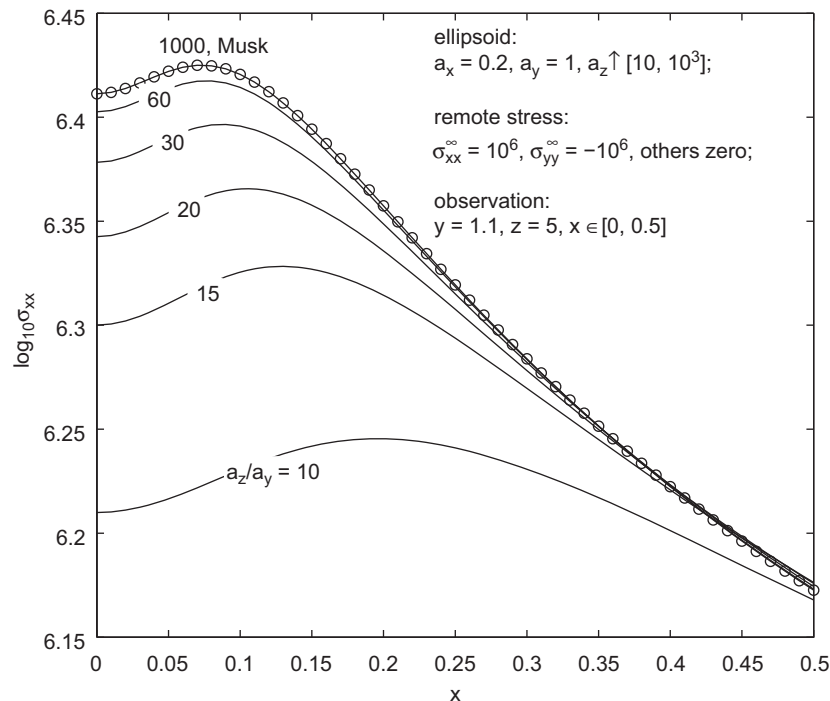

Fig. 3. Stress evolution as an ellipsoid transforms into an elliptical cylinder.

derived the analytical solution. Pollard (1973) presented the computer code for the elastic fields.

We set the remote stress $\sigma_{xx}^{\infty} = 10^6$, $\sigma_{yy}^{\infty} = -10^6$, other components zero, and observe the stress evolution along the route $y = 1.1$, $z = 5$, $x \in [0, 0.5]$. The stress component σ_{xx} by Eshelby and Muskhelishvili (evaluated with Pollard, 1973) are plotted in Fig. 3.

Corresponding displacement perturbations $u_y - u_y^{\infty}$ are plotted in Fig. 4.

Eshelby's solution converges to the elliptical void solution as a_z/a_y increases. When $a_z/a_{x(y)} \geq 10^3$, Eshelby's and Muskhelishvili's solutions are almost identical.

Let us show that when $a_z \gg a_{x(y)}$, a_z has less impact on the elastic field than $a_{x(y)}$ does. Continuing from the *elliptical cylinder*, we let a_x sweep through values around the length of a_y, keeping other conditions the same as above. The elastic field around a circular void was given by Kirsch (1898) and later generalized by
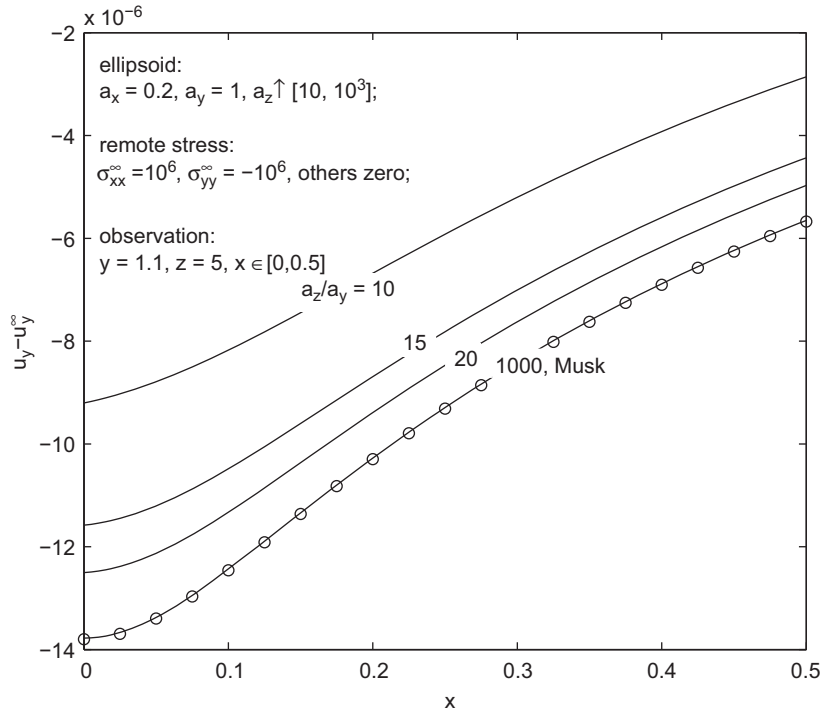

Fig. 4. Displacement perturbations as an ellipsoid transforms into an elliptical cylinder.
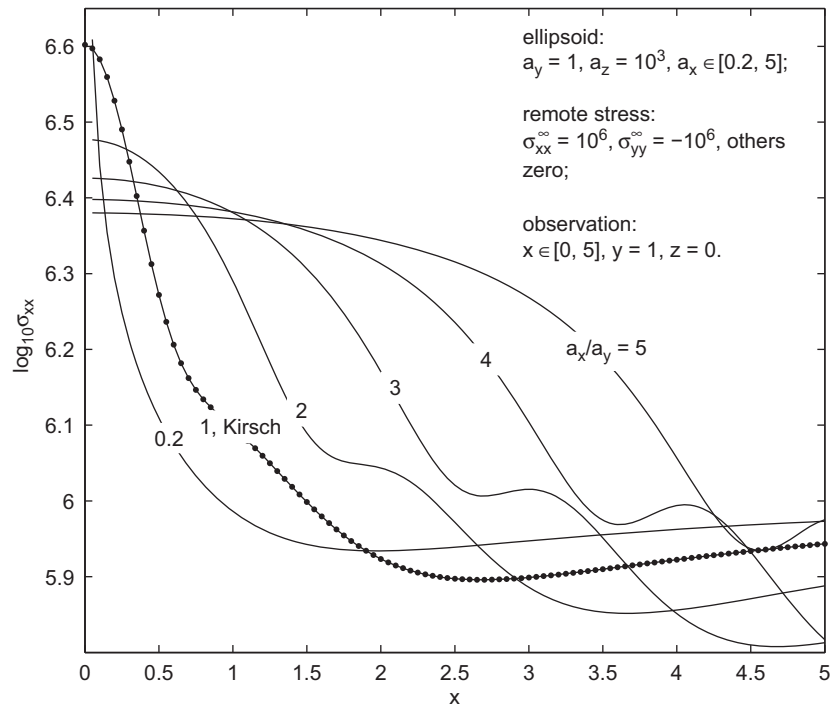

Fig. 5. Stress evolution as an elliptical cylinder transforms into a circular cylinder.

Muskhelishvili (1953). The stress evolution referenced by Kirsch (1898) is plotted in Fig. 5.

As the length of a_x approaches and passes the length of a_y, the stress also approaches, is equal to, and differs from the Kirsch (1898) solution. The impact of transformation $a_z \uparrow [60, 100]$ in Fig. 3 on the stress is much less than the impact of $a_x \uparrow [0.2, 2]$ in Fig. 5.

With the above satisfying validations, we are confident about the code. Finally, let us exploit the strength of Eshelby's solution by using

it to test some well-accepted approximations. Jaeger et al. (2007, pp. 237–242) cite approximations for the stress near a fracture tip given by Maugis (1992), Lardner (1974) and many other publications. Those approximations play important roles in the theory of linear elastic fracture mechanics (Anderson, 2004; Lawn, 1975).

To compare the Eshelby solution to these approximations, we make the elliptical *cylinder* ($a_x \approx a_y$, $a_z \approx 10^3 a_{x(y)}$) *collapse* in the y semiaxes: $a_y \to 0.01 a_x$. The cylindrical void then approaches a planar crack with half length a_x. Under remote (mode I) tension
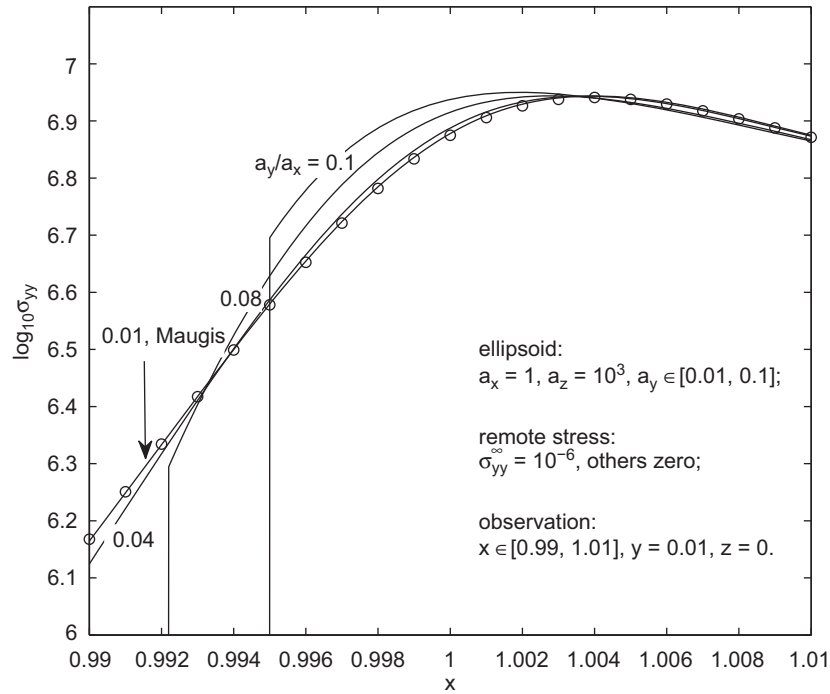

Fig. 6. Stress evolution as a cylindrical void collapses into a planar crack: remote tension.
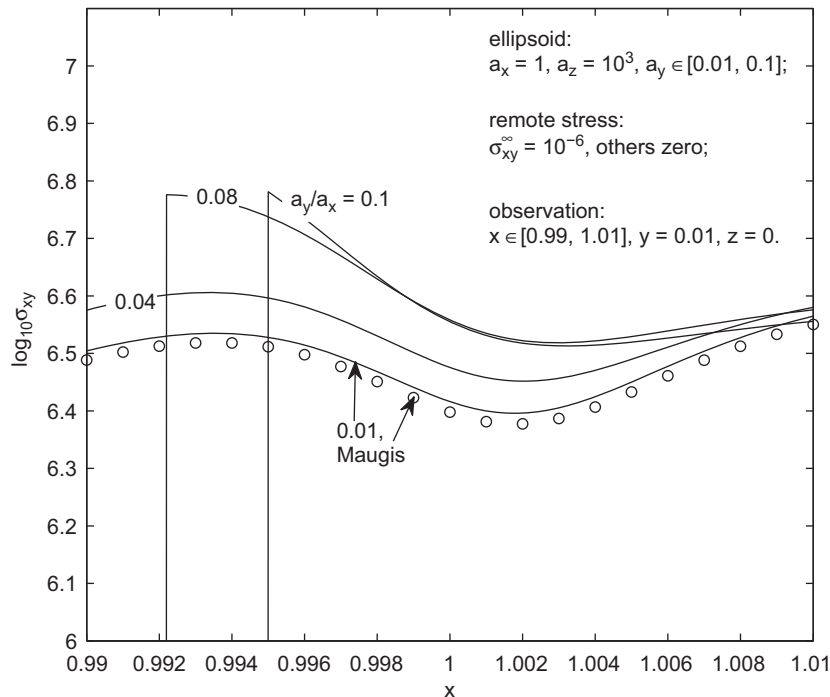

Fig. 7. Stress evolution as a cylindrical void collapses into a planar crack: remote shear mode II.
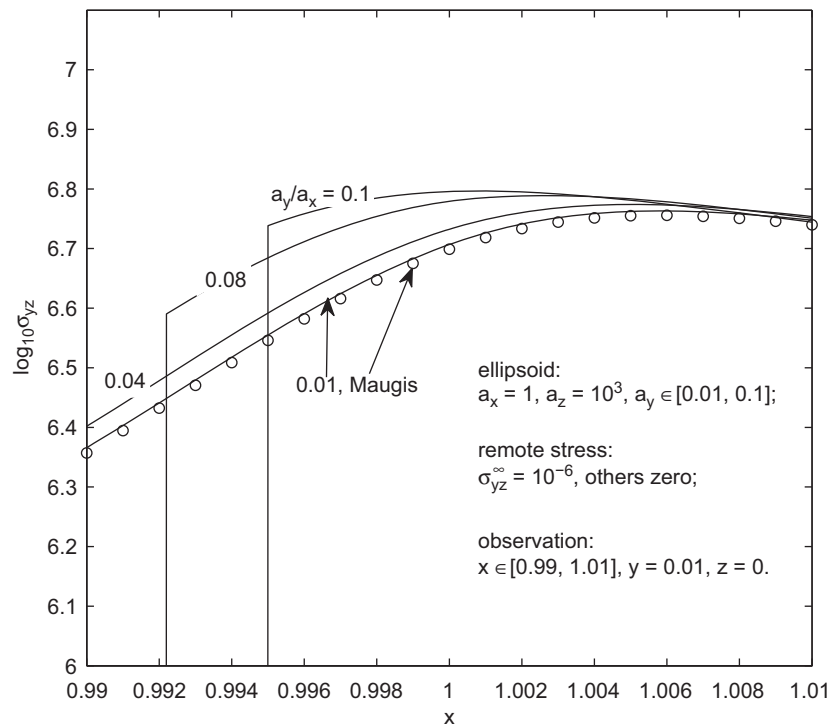
Fig. 8. Stress evolution as a cylindrical void collapses into a planar crack: remote shear mode III.

σ_{yy}^{∞}, or (mode II) shear σ_{xy}^{∞}, the elastic field near the crack tip is approximated by Maugis (1992). The stress approximations cited by Jaeger et al. (2007) neglect the terms of order $r^{1/2}$ and higher, where r is the distance from the observation to the crack tip. Since the stress approximation is only accurate near the crack tip and becomes singular at the tip, we choose an observation route that approaches the tip with a small offset: $y = 0.01$, $z = 0$, and $x \in [a_x - 0.01, a_x + 0.01]$.

First, we apply a remote tension $\sigma_{yy}^{\infty} = 10^6$ and keep other stress components zero. The near-tip σ_{yy} evolution for the transforming cylindrical void is plotted with the Maugis (1992) approximation in Fig. 6.

As a_y/a_x decreases, the void boundary ceases to intercept the observation route, so the sudden stress drop disappears. When $a_y/a_x = 0.01$, the Eshelby solution and the stress approximation agree.

For the same transforming geometry, we apply a mode II remote shear $\sigma_{xy}^{\infty} = 10^6$ and keep other stress components zero. The near-tip σ_{xy} evolution is plotted with Maugis (1992) in Fig. 7.

Similarly to the mode I case, the Eshelby solution approaches the stress approximation. However, when $a_y/a_x = 0.01$, the discrepancy is more noticeable than in Fig. 6. This suggests that the finite a_z has a greater impact on the shear stress perturbation than on the tension perturbation.

Finally, we apply a mode III remote shear $\sigma_{yz}^{\infty} = 10^6$ and keep other stress components zero. The near-tip stress approximation cited in Jaeger et al. (2007) was derived by Lardner (1974). We plot the σ_{yz} evolution with the stress by Lardner (1974) in Fig. 8.

The comparison is similar to Fig. 6, but again with noticeable discrepancy.

7. Conclusion and discussion

For an ellipsoidal inclusion in an isotropic infinite body, we have evaluated *quasi-analytical* expressions for the interior and exterior elastic fields following the Eshelby solution. For an ellipsoidal

inhomogeneity under remote stress, we can simulate the elastic fields by an inclusion problem with a fictitious eigenstrain. A MATLAB code calculates the elastic field of strain, stress, and displacement inside and outside of such an equivalent ellipsoidal inclusion problem.

When we degenerate the ellipsoid into some less general geometries, the code's results converge to the corresponding known solutions. By the geometrical emulations, we find that Eshelby's solution can generalize many special problems into a unified form.

In practice, we can use Eshelby's solution to model geologic structures such as faults, dikes, and compaction bands.

Acknowledgments

Appendix A. Supplementary data

Supplementary data associated with this article can be found in the online version at doi:10.1016/j.cageo.2011.07.008.

References

Anderson, T.L., 2004. Fracture Mechanics: Fundamentals and Applications, third ed. CRC Press, Boca Roton, FL.
Dyson, F.D., 1981. The potentials of ellipsoids of variable densities. Quarterly Journal of Pure and Applied Mathematics 25, 259–288.
Eidelman, A., Reches, Z., 1992. Fractured pebbles—A new stress indicator. Geology 20, 307–310.

Eshelby, J.D., 1957. The determination of the elastic field of an ellipsoidal inclusion, and related problems. Proceedings of the Royal Society of London. Series A. Mathematical and Physical Sciences 241, 376–396.

Eshelby, J.D., 1959. The elastic field outside an ellipsoidal inclusion. Proceedings of the Royal Society of London. Series A. Mathematical and Physical Sciences 252, 561–569.

Eshelby, J.D., 1961. Elastic inclusion and inhomogeneities. Progress in Solid Mechanics 2, 89–140.

Ferrers, N.M., 1877. On the potentials of ellipsoids, ellipsoidal shells, elliptic laminae and elliptic rings of variable densities. Quarterly Journal of Pure and Applied Mathematics 14, 1–22.

Gradshteyn, I., Ryzhik, I., 1965. Table of Integrals, Series, and Products. Academic Press.

Healy, D., 2009. Short note: Elastic field in 3d due to a spheroidal inclusion-MATLAB code for Eshelby's solution. Computers & Geosciences 35, 2170–2173.

Igor, M., 2005. Elliptic Integrals and Functions, MathWork.

Jaeger, J.C., Cook, N.G.W., Zimmerman, R., 2007. Fundamentals of Rock Mechanics, fourth ed. Wiley–Blackwell.

Jiang, D., 2007. Numerical modeling of the motion of deformable ellipsoidal objects in slow viscous flows. Journal of Structural Geology 29, 435–452.

Katsman, R., 2010. Extensional veins induced by self-similar dissolution at stylolites: analytical modeling. Earth and Planetary Science Letters 299, 33–41.

Kirsch, G., 1898. Die theorie der elastizitat und die bedürfnisse der festigkeitslehre. Zeitschrift des Verlines Deutscher Ingenieure 42, 797–807.

Lardner, R.W., 1974. Mathematical Theory of Dislocations and Fracture. University of Toronto Press.

Lawn, B.R., 1975. Fracture of Brittle Solids, Cambridge Solid State Science Series. Cambridge University Press, Cambridge, UK.

Maugis, D., 1992. Adhesion of spheres: the jkr–dmt transition using a Dugdale model. Journal of Colloid and Interface Science 150, 243–269.

Mura, T., 1987. Micromechanics of Defects in Solids: Mechanics of Elastic and Inelastic Solids. Kluwer Academic.

Muskhelishvili, N., 1953. Some Basic Problems of the Mathematical Theory of Elasticity. Kluwer Academic.

Pollard, D.D., 1973. Equations for stress and displacement fields around pressurized elliptical holes in elastic solids. Mathematical Geology 5, 11–25. doi:10.1007/BF02114084.

Reches, Z., 1998. Tensile fracturing of stiff rock layers under triaxial compressive stress states. International Journal of Rock Mechanics and Mining Sciences 35 (4–5).

Routh, E.J., 1895. Theorems on the attraction of ellipsoids for certain laws of force other than the inverse square. Philosophical Transactions of the Royal Society of London. Series A 186, 897–950.

Rudnicki, J.W., 1977. The inception of faulting in a rock mass with a weakened zone. Journal of Geophysical Research 82 (5).

Sharma, P., Ganti, S., 2004. Size-dependent Eshelby's tensor for embedded nano-inclusions incorporating surface/interface energies. Journal of Applied Mechanics 71, 663–671.